이학석사학위논문

이리듐 복합체를 이용한 인광 및 전기화학 발광 기반의 수은 이온 검출용 듀얼 프로브

Ir(III) Complex–based Phosphorescence and Electrogenerated Chemiluminescence Dual–probe for the Detection of Mercury Ion

2018 년 2 월

서울대학교 대학원

화학부 유기화학 전공

이 하 영

이리듐 복합체를 이용한 인광 및 전기화학 발광 기반의 수은 이온 검출용 듀얼 프로브

Ir(III) Complex–based Phosphorescence and Electrogenerated Chemiluminescence Dual–probe for the Detection of Mercury Ion

지도교수 홍 종 인

이 논문을 이학석사학위 논문으로 제출함.

2018 년 **2** 월

서울대학교 대학원 화학부

유기화학전공

이 하 영

이하영의 이학 석사 학위논문을 인준함.

2018 년 **2** 월

위 원 장 정 영 근 (인)

부 위 원 장 홍 종 인 (인)

위 원 이 동 환 (인)

Abstract

Ir(III) Complex–based Phosphorescence and Electrogenerated Chemiluminescence Dual–probe for the Detection of Mercury Ion

Hayoung Rhee

Major in Organic Chemistry

Department of Chemistry

Graduate School

Seoul National University

Mercury, one of the most prevalent toxic metal elements, poses severe risks for human health and environment. Thus, various molecular probes have been developed for the colorimetric and fluorometric detection of mercury. Nevertheless, it is still urgent to develop a cost effective, rapid, selective and sensitive probe for the detection of mercury(II) ion.

In this study, we designed several Ir(III) complex–based phosphorescence and electrochemiluminescence dual mode chemodosimeters, which possess phenylpyridine (ppy) or phenylisoquinoline (piq) as main ligands and acetylacetone as ancillary ligands in common for the selective detection of mercury(II) ion.

Acetylacetonate ancillary ligand of probe **1** reacted with mercury(II) ion selectively, inducing phosphorescence enhancement with concomitant blue shift of the emission spectra. Meanwhile, mercury(II) ion selectively quenched the phosphorescence of probe **2**. In addition, we proposed a two–step sensing mechanism through the comparison of NMR spectra of the probes in the absence and presence of mercury(II) ion. Mass analysis and crystallographic determination further supported that acetylacetonate readily reacts with mercury(II) ion, followed by the dissociation of mercury–acetylacetone from Ir(III) complex.

These probes further showed selective electrogenerated chemiluminescence (ECL) responses, quenching upon the addition of mercury(II) ion. ECL based chemosensors have been widely studied for their several advantages, such as the possibility of being a powerful candidate for point–of–care (POC) detection, high sensitivity and simple analytical process. Moreover, probe **9** showed the best ECL property with a good linear correlation between 0 and 40 μM of mercury(II) ion with a low limit of detection (LOD) as 170 pM.

Keywords: Cyclometalated Ir(III) Complex, Acetylacetone, Chemodosimeter, Phosphorescence, Electrogenerated Chemiluminescence (ECL), Dual mode, Mercury(II) ion

Student Number: 2016–20358

Contents

A. Background

A.1. The Fundamentals of Fluorescence Sensors

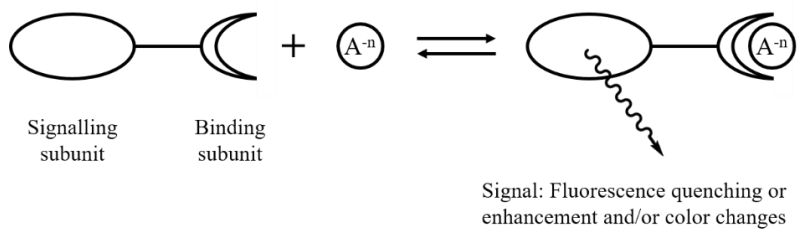

Figure 1. Anion chemosensors based on the binding site–signaling subunit approach.

Many chemical sensors follow the approach of the covalent attachment of signaling and binding subunits[1] (Fig. 1). The binding subunit of a chemosensor is a site that can accommodate chemical species by noncovalent interactions. The noncovalent interactions in the binding site usually utilize electrostatic attractions, hydrogen bonding and coordination to metal ions. The role of the signaling subunit is to translate chemical information taking place at the molecular level into an observable signal. For example, rhodamine, pyrene, bodipy, fluorescein are well–known fluorophores that are commonly employed as signaling units.

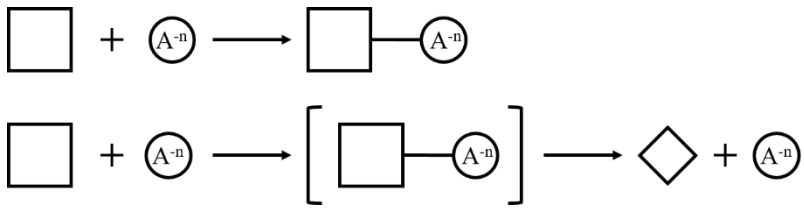

Figure 2. Schematic diagram of chemodosimeter. An anion reacts with chemodosimeter and remains covalently attached or catalyzes a chemical reaction.

Chemodosimetric approach, on the other hand, involves the use of specific chemical transformations induced by the presence of target molecules (Fig. 2). This covalent bonding approach is generally irreversible, presenting some advantages, such as highly selective reactivity and possibility to reflect accumulative responses related directly to the concentration of the analytes.

Fluorogenic Principles of Sensing

Fluorescence detection has been used extensively as a versatile tool in analytical chemistry, biochemistry, cell biology, etc.[2] There are several fluorogenic principles of sensing analytes. Generally, an electron in the ground state absorbs light, which induces the excitation to the lowest unoccupied molecular orbital (LUMO) and then goes to the highest occupied molecular orbital (HOMO), releasing the excess of energy as light. This process could either be disturbed or accelerated by several mechanisms.

First, photoinduced electron transfer (PeT) is one of the most commonly applied mechanisms to modulate fluorescence property[3] (Fig. 3). After an electron absorbs light and excites to a higher energy level, the electron can migrate to an

orbital of another part of a molecule or another electron can occupy the orbital which was originally a ground state to block the emission of light. In other words, fluorescence quenching occurs because the transition from the excited to the ground state takes place following a nonradiative path.

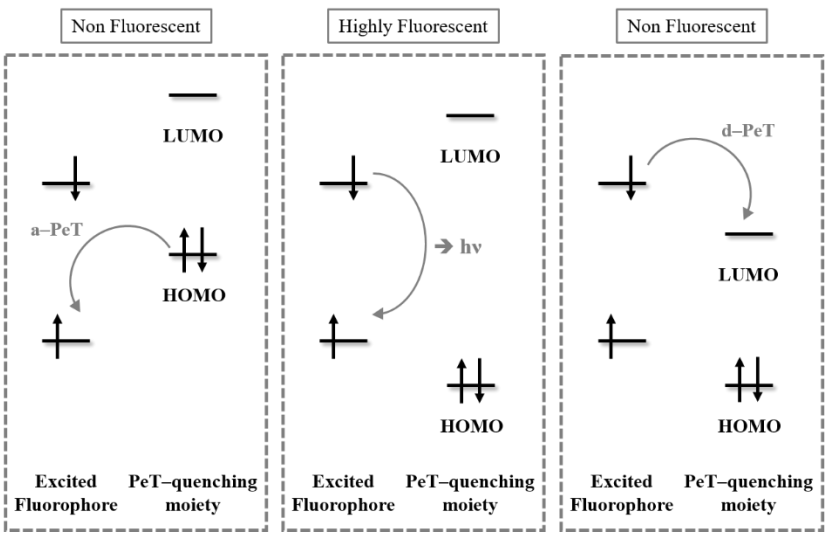

Figure 3. Schematic molecular orbital diagram of the fluorescence off/on switch including the PeT process.

Second, Förster Resonance Energy Transfer (FRET) is a nonradiative process in which an excited dye donor (usually a fluorophore) transfers energy to a dye acceptor in the ground state through long–range dipole–dipole interactions[4] (Fig. 4). To design FRET–based ratiometric fluorescent probes, some design criteria involving energy donors, acceptors, and linkers should be considered. (1) The absorption spectrum of the donor should be separated from that of the acceptor in order to ensure independent excitation at the absorption wavelengths of the donor

and acceptor, respectively. (2) The emission spectrum of the donor should be resolved from that of the acceptor for high accuracy in the measurement of fluorescence intensity ratios. (3) The donor fluorophore and the acceptor dye should have comparable brightness, which may impart two well–separated emission bands with comparable intensities before and after the interaction with an analyte. (4) Appropriate linkers are needed to avoid static fluorescence quenching due to close contact of donor and acceptor dyes in aqueous environment. (5) A near perfect energy transfer efficiency should be achieved in the energy transfer platform.

Moreover, intramolecular charge transfer (ICT), excited state intramolecular proton transfer (ESIPT), formation of excimer, etc. are also commonly exploited sensing mechanisms for the design of ratiometric fluorescent probes.

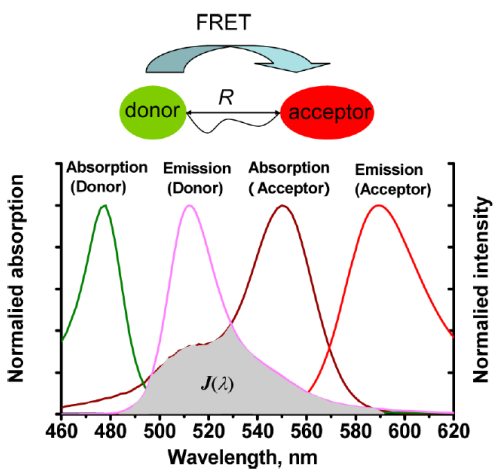

Figure 4. Schematic of the Förster Resonance Energy Transfer (FRET) process. This figure was adapted from reference 11 with permission. Copyright 2013 American Chemical Society.

A.2. Principles of Electrochemiluminescence (ECL)

Electrochemiluminescence, also called electrogenerated chemiluminescence or ECL, involves the generation of radical species at electrode surfaces, which undergo electron transfer reactions to form excited states that generate light.[5] The first detailed ECL studies were reported by Hercules and Bard et al,[6–8] in the mid–1960s, and now it has become a very powerful analytical technique.[9]

ECL has attracted much attention because it provides several advantages over conventional analytical tools. ECL requires no extra light source, offering the possibility of miniaturizing the detection device and allowing point–of–care (POC) detection as a result. Furthermore, electrochemistry enables highly sensitive method and no background signals with low limit of detection.[10]

General Reaction Mechanisms

Conventional reaction mechanism of ECL known as "annihilation", involves electron transfer reaction between an oxidized and a reduced species, both of which be generated at an electrode by alternate pulsing of the electrode potential. The general annihilation mechanism is stated below:

$$\mathrm{A} + \mathrm{e}^- \rightarrow \mathrm{A}^{-\bullet} \text{ (Reduction at electrode)}$$

$$\mathrm{A} - \mathrm{e}^- \rightarrow \mathrm{A}^{+\bullet} \text{ (Oxidation at electrode)}$$

$$\mathrm{A}^{-\bullet} + \mathrm{A}^{+\bullet} \rightarrow \mathrm{A}^* + \mathrm{A} \text{ (Excited state formation)}$$

$$\mathrm{A}^* \rightarrow \mathrm{A} + \mathrm{h}\nu \text{ (Light emission)}$$

This process can occur only when the ECL emitter (A) produces stable radical cation ($A^{+\bullet}$) and radical anion ($A^{-\bullet}$) sufficiently.

In addition, it is possible to generate ECL in a single potential step using a coreactant. A coreactant is a compound that can produce a reactive intermediate, such as a strong reducing or oxidizing agent, when appropriate potential is applied. For example, oxalate ion ($C_2O_4^{2-}$) was the first coreactant discovered by Bard's group.[11] Through this typical coreactant ECL system, the strong reductant, $CO_2^{-\bullet}$, produced by the oxidation of $C_2O_4^{2-}$, oxidizes the luminophore and this process is often referred to "oxidative–reduction" process. Another important example of an "oxidative–reduction" coreactant is tri–*n*–propylamine (TPA, $(CH_3CH_2CH_2)_3N$). The key reaction steps for general ECL luminophores with TPA are outlined below:

$$M - e^- \rightarrow M^{+\bullet}$$

$$TPA - e^- \rightarrow TPA^{+\bullet}$$

$$M^{+\bullet} + TPA \rightarrow M + TPA^{+\bullet}$$

$$TPA^{+\bullet} \rightarrow TPA^{\bullet} + H^+$$

$$M^{+\bullet} + TPA^{\bullet} \rightarrow M^* + side\ product$$

$$M + TPA^{\bullet} \rightarrow M^{-\bullet} + side\ product$$

$$M^{-\bullet} + M^{+\bullet} \rightarrow M^* + M$$

$$M^{-\bullet} + TPA^{+\bullet} \rightarrow M^* + TPA$$

$$M^* \rightarrow M + h\nu$$

The oxidation of TPA can occur via a "catalytic route" where $M^{+\bullet}$ reacts with TPA as well as by direct reaction of TPA at the electrode.[12] Upon the oxidation, TPA initially produces a short–lived $TPA^{+\bullet}$, which rapidly deprotonates to generate a strongly reducing radical species $TPA^{\bullet}$.[13] Then this $TPA^{\bullet}$ reacts with $M^{+\bullet}$ to form an excited–state species, M^*.

A.3. Mercury(II) Ion Sensors

Heavy metal ions are of great concern, not only among chemists, biologists and environmentalists, but also increasingly among the general population who are aware of many disadvantages associated with them. Especially, mercury is one of the most toxic ions known that does not have any vital or beneficial effects and therefore is consistently receiving considerable attention.[14]

Traditional quantitative analysis of mercury(II) ion employ several methods, including mass spectrometry, gas chromatography and plasma atomic emission spectrometry. However, these techniques often require expensive equipment and involve sophisticated and time–consuming procedures. Alternatively, fluorescence technology has been studied widely owing to its simplicity, sensitivity and simple manipulation. Thus, during the last couple of decades, considerable efforts have been made to develop small–molecule fluorescent sensors that can selectively detect mercury(II) ion.[15, 16]

Some of the notable strategies for selective detection of mercury(II) ion are as follows and depicted in Fig. 5. Soto et al. developed a chromogenic macrocycle reagent, which converts its color from red to yellow in the presence of mercury(II) ion (Fig. 5a).[17] In 2000, Savage et al. studied a series of macrocyclic ligands with appended chromophores and fluorophores for selective metal ion chemosensors (Fig. 5b).[18] While the majority of the probes are based on the coordination of multiple nitrogen, oxygen and sulfur atoms to metal ion, in 2008, Koide et al.[19] described a new methodology based on the reactivity of mercury(II) ion with alkynes. They

showed that the fluorescence intensity of fluorescein with an alkyne functional group was enhanced by oxymercuration followed by β–elimination reaction (Fig. 5c). Kim et al.[20] reported a coumarin–derived alkyne based luminescent probe operating in the presence of substoichiometric amounts of mercury(II) ion (Fig. 5d).

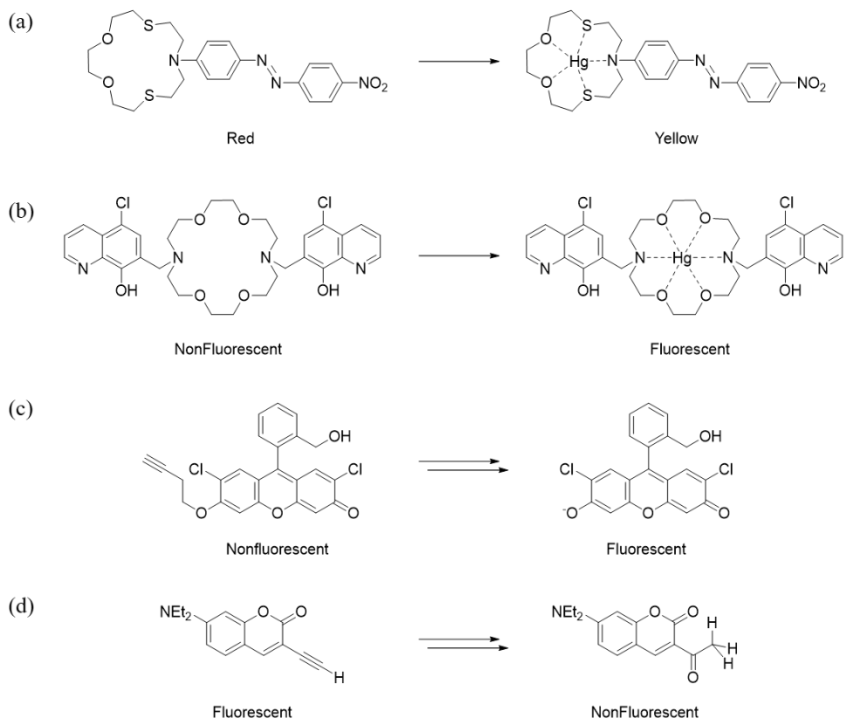

Figure 5. Examples of various sensing strategies for the detection of mercury(II) ion.

As shown in Fig. 6[21], a molecular beacon was reported for re–usable electrochemical sensor for mercury(II) ion. Recognition of mercury(II) ion by T (thymine)–Hg^{2+}–T complex formation induced a conformational change of the molecular beacon into a hairpin structure. This folding brought dangling ferrocene

into a close proximity with an electrode surface, causing an electron transfer and generating current.

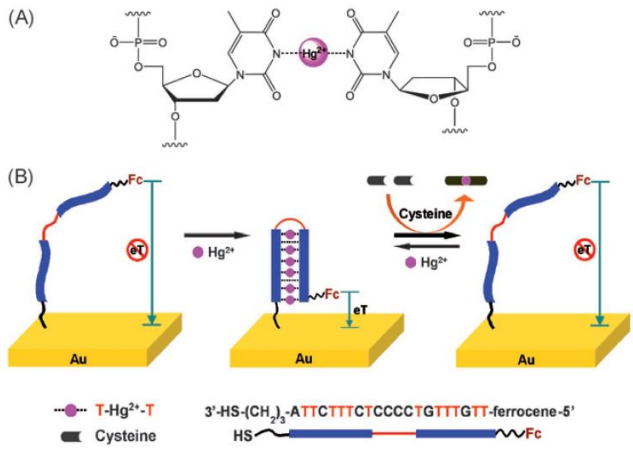

Figure 6. (A) Formation of T–Hg^{2+}–T base pair. (B) Schematic description of the electrochemical sensor for Hg^{2+} ion detection. This figure was adapted from reference 39 with permission. Copyright 2009 The Royal Society of Chemistry.

A.4. Excited State Photophysics of Cyclometalated Ir(III) Complexes

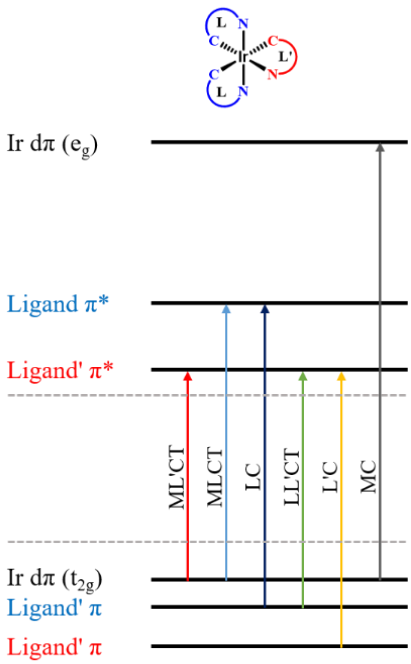

Figure 7. The construction of excited states via molecular orbital interactions: MC, metal–centered ligand–field state; LC, ligand–centered state; MLCT, metal–to–ligand charge–transfer state; LL'CT, ligand–to ligand charge–transfer state; L and L' denote different ligands of a heteroleptic Ir(III) complex.

The photophysical processes of typical heteroleptic Ir(III) complexes are schematically depicted in Fig. 7. The phosphorescence emission of iridium complexes arise from the population of the ligand–centered (LC) and metal–to–ligand charge–transfer (MLCT, Ir → ligand) transition states. In addition to these transitions, strong spin–orbit coupling (SOC) exerted by the iridium core facilitates

transitions of singlet MLCT and LC to triplet states, yielding four electronic states: the singlet and triplet MLCT (^{1}MLCT and ^{3}MLCT) or LC (^{1}LC and ^{3}LC) transition states. This phenomenon occurs because the singlet transition state undergoes highly efficient intersystem crossing to the triplet transition state. MLCT and LC electronic states are strongly coupled because they share a common LUMO located on the cyclometalated ligand.[22, 23]

B. Cyclometalated Ir(III) Complex–based Chemodosimeters for Mercury(II) Ion

B.1. Photoluminescence–based Probes

B.1.1. Introduction

Mercury is one of the most prevalent toxic metal elements, which poses severe risks for human health and the environment. Mercury easily passes through biological membranes such as skin, respiratory, and gastrointestinal tissues, leading to digestive, cardiac, kidneys, and lung damages and especially permanent damage to the central nerve system. The gradual accumulation of mercury in human body also induces Hunter–Russell syndrome, Alzheimer's and Minamata disease.[24]

According to numerous researches, fluorescent small molecule based sensors offer an attractive approach to trace neurotoxic mercury(II) ion. In 1970s, several papers about acetylacetone derivatives of mercury(II) ion were reported.[25–28] In addition, some mercury(II) ion probes based on Ir(III) complexes, that were predicted to have some kind of reaction between mercury(II) ion and acetylacetone have been published, successively.[29, 30] However, no exact mechanism or any crystallographic determination were discovered to date.

Herein, we report acetylacetonato Ir(III) complexes for the selective detection of mercury(II) ion via phosphorescence and electrogenerated chemiluminescence dual techniques and their mercury(II) ion sensing mechanism through ^{1}H NMR, mass spectra and crystal data.

B.1.2. Results and Discussion

Spectroscopic property

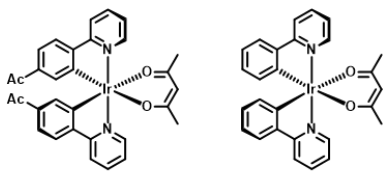

1 2

The photophysical properties of the probes **1** and **2** were investigated using UV–Vis absorption and photoluminescence spectroscopies including titration studies with mercury(II) ion. As shown in Fig. 8, the phosphorescence intensity of **1** (10 μM in acetonitrile/water = 9/1, λ_{ex} = 400) increased gradually with concomitant blue shift from 600 nm to 521 nm. The enhancement reached plateau, after the addition of 3 equivalents of mercury(II) ion. It is worth noting that the spectroscopic change occurred almost instantaneously. We also found that the phosphorescence changed in a stepwise manner. The ratio of the intensity at 521 nm to that at 600 nm (I_{521}/I_{600}) showed only a small change when 3–9 μM of the mercury(II) ion was added, followed by a stiff–enhancing region of 9–30 μM of mercury(II) ion. A good linear relationship between the phosphorescence intensity ratio and the mercury(II) ion concentration was observed in the stiff–enhancing region (9–30 μM), which had a higher coefficient of determination (R^2) value than that of **2**. The estimated limit of detection (LOD) was as low as 73 nM.

Meanwhile, the phosphorescence intensity of **2** (10 μM in acetonitrile/water = 9/1, λ_{ex} = 400) decreased at 525 nm until 4 equivalents of mercury(II) ion was added (Fig. 9). **2** as well showed a small change when 3–9 μM of mercury(II) ion was added and revealed a gradual decrement after the addition of 12–40 μM of mercury(II) ion. A 35–fold decrement proposed LOD of 160 nM. Again, the spectral changes were found to be instantaneous after the addition of mercury(II) ion.

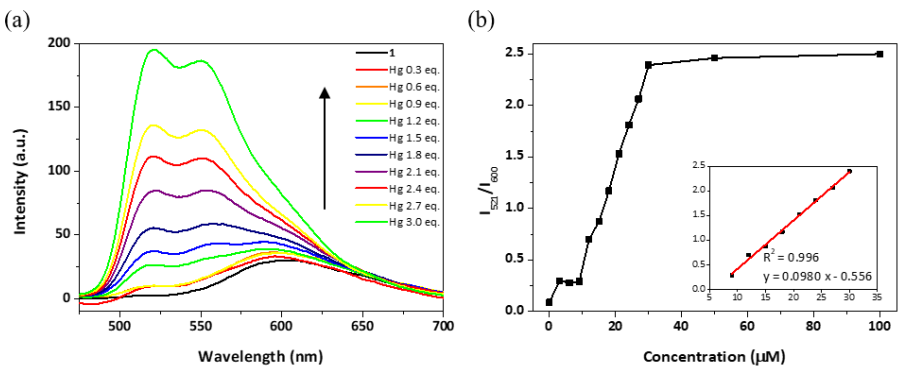

Figure 8. (a) Titration curves of **1** (10 μM) in the presence of various amounts of Hg^{2+} ion (0–30 μM, instant) in CH_3CN/water (9/1). (b) Phosphorescence intensity changes of **1** (10μM) upon the addition of Hg^{2+} ion (0–100 μM). Inset: Plot of I_{521}/I_{600} vs [Hg^{2+}] (9–30 μM) showing the linear relationship. LOD = 73 nM.

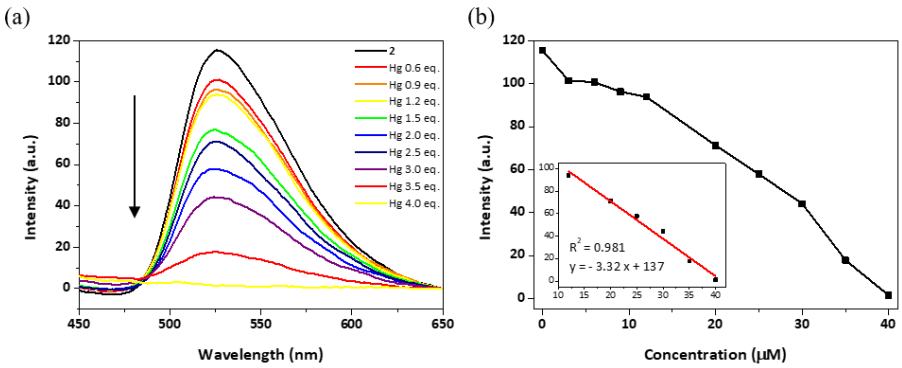

Figure 9. (a) Titration curves of **2** (10 μM) in the presence of various amounts of Hg^{2+} ion (0–40 μM, instant) in CH_3CN/water (9/1). (b) Phosphorescence intensity changes of **2** (10 μM) upon the addition of Hg^{2+} ion (0–40 μM). Inset: Plot of I_{525} vs [Hg^{2+}] (12–40 μM) showing the linear relationship. LOD = 160 nM.

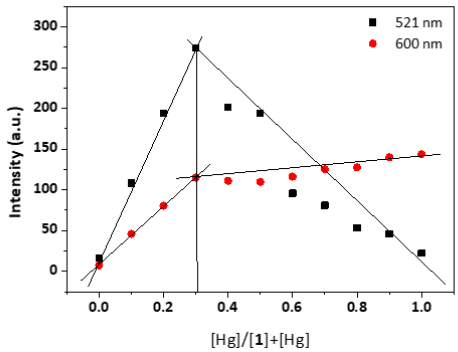

Figure 10. Job's plot for **1** and Hg^{2+} ion at 521 nm and 600 nm in CH_3CN/water (9/1). [**1**] + [Hg^{2+}] = 5.0 x 10^{-5} mol L^{-1}. λ_{ex} = 400 nm.

On the basis of the Job's plot experiment, the binding ratio between the probe and mercury(II) ion was confirmed (Fig. 10). It exhibited maximum

phosphorescence intensity near mole fraction of 0.33, which implies 2:1 binding stoichiometry of the probe to mercury(II) ion.

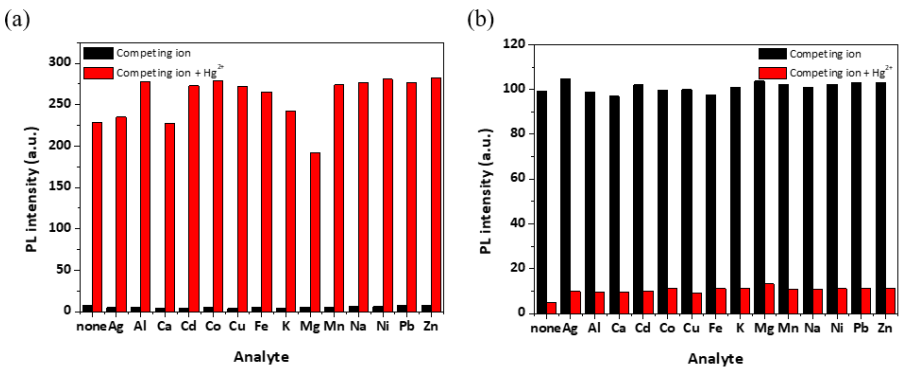

Figure 11. Phosphorescence responses of (a) **1** (10 μM) and (b) **2** (10 μM) to 50 μM of various metal ions (black) and additional 50 μM of Hg^{2+} ion (red).

Selectivity Test

Competition assay was performed to further evaluate the interference of other metal ions (Fig. 11). The phosphorescence intensities of **1** and **2** in the presence of various metal ions (50 μM), such as Ag^{+}, Al^{3+}, Ca^{2+}, Cd^{2+}, Co^{2+}, Cu^{2+}, Fe^{2+}, K^{+}, Mg^{2+}, Mn^{2+}, Na^{+}, Ni^{2+}, Pb^{2+}, and Zn^{2+}, were nearly the same, indicating that these chemodosimeters display high selectivity toward mercury(II) ion. Then, in the presence of competing ions, 50 μM of mercury(II) ion was treated additionally and it brought the enhancement and decrement of the phosphorescence of **1** and **2**, respectively, implying that the other cations cannot interfere the reaction between **1**, **2** and mercury(II) ion. In addition, the reason of the phosphorescence changes

seemed hardly related to the metal coordination since zinc ion, known as a good Lewis acid, did not react with the probes.

Mass analysis

Then we carried out ESI–MS and MALDI–TOF analysis to confirm the product formed after the addition of mercury(II) ion. Before adding mercury(II) ion, molecular ion peaks of **1** and **2** appeared at 684.218 and 600.116 (m/z), respectively. After the addition of even a small amount of mercury(II) ion (0.5 equivalent) the molecular ion peaks completely disappeared. In the case of **2**, the major peak appeared at 501.093 (m/z), which corresponds to $(ppy)_2Ir^+$. In addition, the minor peak was shown at 542.120 (m/z), representing $(ppy)_2Ir^+(CH_3CN)$. Mass spectral data of **1** was similar to that of **2**. The major peak appeared at 585.114 (m/z) which corresponds to $(Acppy)_2Ir^+$ (Ac = acetyl) and the additional minor peak at 626.141 (m/z), which represents $(Acppy)_2Ir^+(CH_3CN)$.

Control experiments

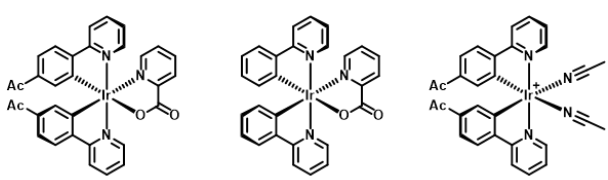

Inspired by MS results, we synthesized two additional compounds, $(Acppy)_2Ir(pic)$ (**3**) and $(ppy)_2Ir(pic)$ (**4**) (pic = picolinic acid) to confirm whether acetylacetonate

ligand is associated with the reaction with mercury(II) ion. As expected, phosphorescence of these two picolinato Ir(III) complexes did not show any spectral changes even after the addition of 10 equivalents of mercury(II) ion (Fig. 12). These results clearly showed that acetylacetone is responsible for the reaction with mercury(II) ion.

Furthermore, we synthesized $(Acppy)_2Ir(CH_3CN)_2$ (**5**) from the dimer form of Acppy (see Experimental Section). As shown in Fig. 13, the phosphorescence spectrum was found to be almost identical to that of **1** treated with mercury(II) ion, indicating that the reaction of **1** with mercury(II) ion results in the decomposition to $(Acppy)_2Ir(CH_3CN)_2$, and this decomposition process is a key of the sensing mechanism.

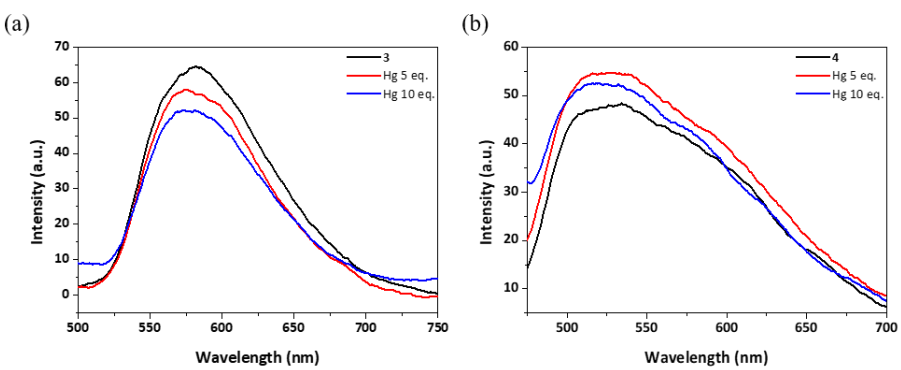

Figure 12. Phosphorescence intensity changes of (a) **3** (10 μM) and (b) **4** (10 μM) upon the addition of Hg^{2+} ion (0–100 μM).

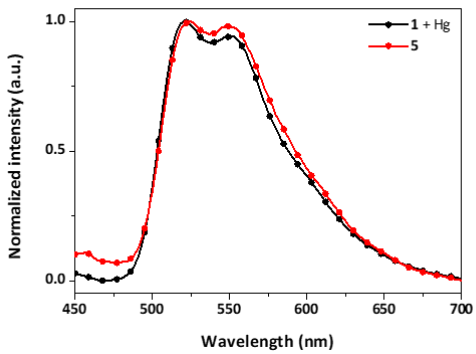

Figure 13. Normalized phosphorescence intensity of **1** upon the addition of 50 μM of Hg^{2+} ion and **5**.

Crystallography

No crystal structure determination of Ir(III) complex reacted with mercury(II) ion has been published to date. As shown in Fig. 14, the structure of $(ppy)_2Ir^+$ complex was unambiguously revealed on the basis of a single crystal X–ray diffraction analysis.[31] It is definite that acetylacetone of the Ir(III) complex was detached right after the addition of mercury(II) ion, forming cationic Ir(III) complex and acetylacetone–mercury complex as a result.

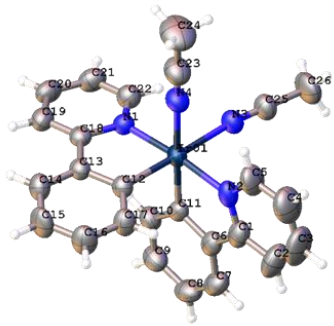

Figure 14. Single crystal X–ray structure of **2** after the addition of 0.5 equivalent of Hg^{2+} ion (thermal ellipsoids are drawn at 50% probability level). Color code: C, grey; N, blue; H, white; Ir, dark blue.

NMR study

In order to gain deeper understanding about the sensing mechanism, NMR spectroscopic experiments in CD_3CN were performed. As shown in Fig. 15, H_a proton (5.3 ppm) of **1** clearly disappeared, whereas H_b protons (1.76 ppm) shifted downfield. In addition, the NMR spectrum of **1** in the presence of mercury(II) ion was very similar to that of **5**, which was also shown in the control experiments (Fig. 13). **2** showed a similar pattern change of the NMR spectrum after the addition of mercury(II) ion (Fig. 16). We confirmed that the shifted H_b protons appeared at the same position as the mixture of acetylacetone and mercury(II) ion.

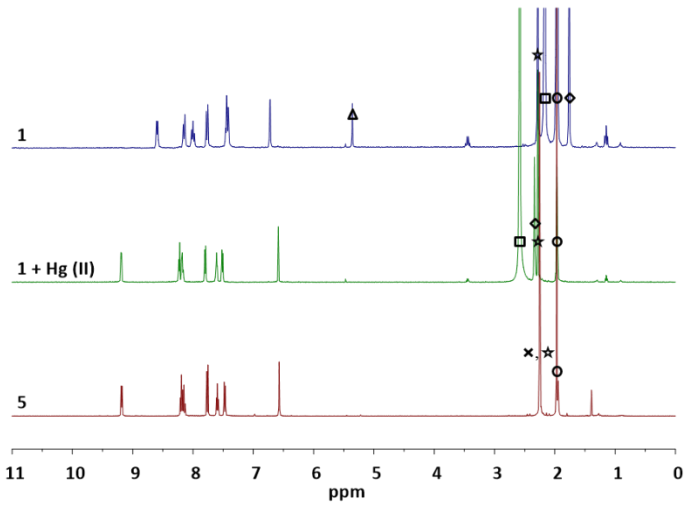

Figure 15. Comparison of NMR spectra of **1**, **1** + 5 equivalents of Hg^{2+} ion and **5**.

○: acetonitrile (solvent), □: water, △: H_a, ◇: H_b, ☆: acetyl–H, ×: CH_3CN (Ir coordinated)

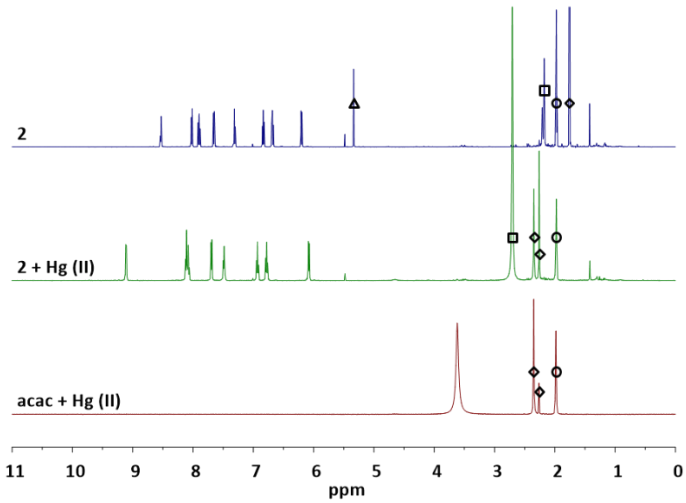

Figure 16. Comparison of NMR spectra of **2**, **2** + 5 equivalents of Hg^{2+} ion and acetylacetone + 5 equivalents of Hg^{2+} ion. ○: acetonitrile (solvent), □: water, △: H_a, ◇: H_b

The Job's plot for **1** and mercury(II) ion (Fig. 10) revealed that a mercury(II) ion tends to coordinate with two acetylacetonate ligands. Besides, a single crystal structure of mercury(II) coordinating with two molecules of 2,2,6,6–tetramethyl–3,5–heptanedione has been reported.[26–28,32,33] Therefore, we propose a two–step sensing mechanism. In the first step, acetylacetonate readily reacts with mercury(II) ion, inevitably forming tetrahedral carbon center and β–diketone structure, which has weaker coordinating ability. Then, the β–diketone rapidly dissociates from Ir(III) complex to generate cationic Ir(III) complex as shown in Scheme 1.

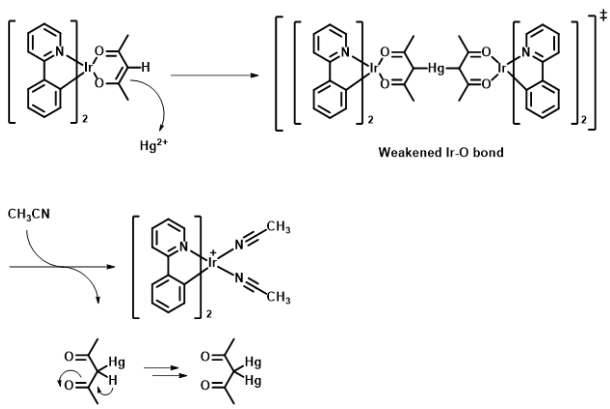

Scheme 1. The expected sensing mechanism of acetylacetonato Ir(III) complexes for Hg^{2+} ion.

B.1.3. Conclusion

We developed new phosphorescence chemodosimeters based on Ir(III) complex for the selective detection of mercury(II) ion. The phosphorescence intensities were enhanced or suppressed by the association of mercury(II) ion for the probes **1** and **2**, respectively. In addition, we uncovered the sensing mechanism that acetylacetonate

rapidly reacts with mercury(II) ion, inevitably inducing the dissociation of acetylacetonate–mercury structure from the original Ir(III) complex.

B.1.4. Experimental Section

Materials and methods

All the chemicals were purchased from Sigma–Aldrich Corp., Tokyo Chemical Industry and Acros Organics and were used without further purification. Analytical thin layer chromatography was performed using Merck silica gel 60 F254 on aluminium foil. SiliaFlash® P60 (230–400 mesh) from SILICYCLE was used for stationary phase in chromatographic separation. All the ^{1}H and ^{13}C NMR spectra were obtained using Bruker Advance DPX–300 or Agilent 400–MR DD2 Magnetic Resonance System. Chemical shifts (δ) were reported in ppm (in $CDCl_3$, CD_3CN or DMSO–d_6). Absorption spectra were recorded on Beckman DU 800 Series and fluorescence emission spectra were measured in JASCO FP–6500 spectrometer. The solutions of the probes **1**, **2** and **9** for all the photophysical experiments were prepared in 2 mM stock solution in DMSO and stored in a refrigerator for further use.

Synthesis of compounds

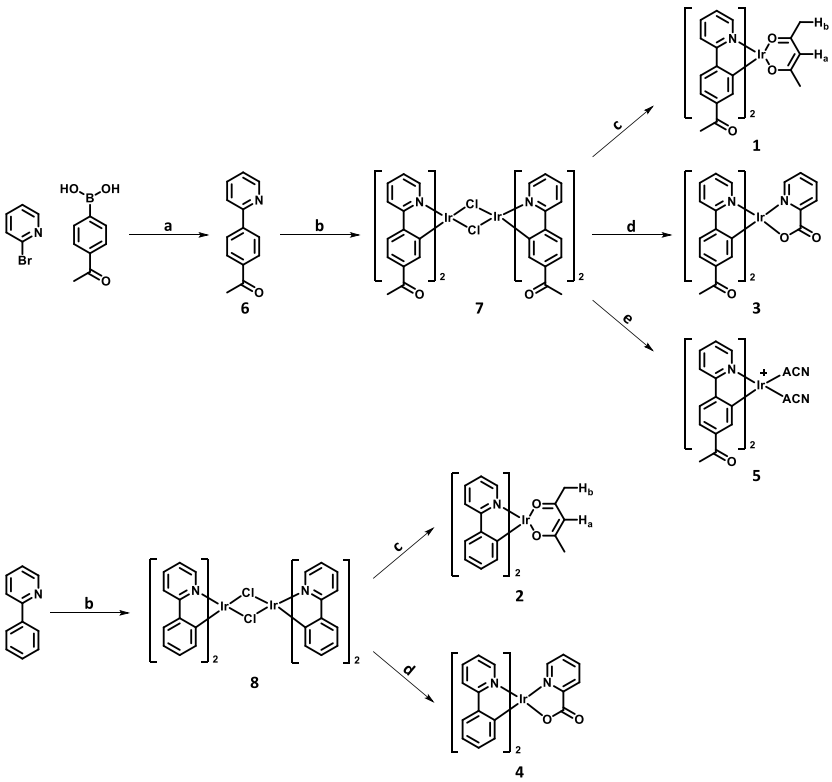

Scheme 2. a) $Pd(PPh_3)_4$, K_2CO_3, THF, H_2O, reflux; b) $IrCl_3 \cdot xH_2O$, 2–ethoxyethanol, H_2O, reflux; c) acetylacetone, Na_2CO_3, 2–ethoxyethanol, 50 °C; d) picolinic acid, Na_2CO_3, 2–ethoxyethanol, 50 °C; e) $AgBF_4$, acetonitrile, reflux. (THF = tetrahydrofuran)

Synthesis of 6

4–Acetylphenyl boronic acid (892 mg, 5.44 mmol), 2–bromopyridine (660 mg, 4.18 mmol), tetrakis(triphenyl phosphine)palladium (144 mg, 0.125 mmol) and K_2CO_3 (1733 mg, 12.5 mmol) were dissolved in THF (15 mL) and H_2O (15 mL). The mixture was refluxed at 80 °C for 5 h and was cooled down to room temperature. The residue was extracted with CH_2Cl_2 and the organic layer was dried over

anhydrous Na_2SO_4, filtered and evaporated under reduced pressure to afford the crude product. Then it was purified by silica gel column chromatography with hexane and ethyl acetate. The product was obtained as a white solid with an isolated yield of 72 % (580 mg). ^{1}H NMR (300 MHz, $CDCl_3$, δ): 9.23 (dd, J = 0.8, 2.3 Hz, 1H), 9.29 (dd, J = 2.3, 8.3 Hz, 1H), 8.09–8.06 (m, 2H), 7.85 (dd, J = 0.8, 8.3 Hz, 1H), 7.54–7.47 (m, 3H), 2.67 (s, 3H).

Synthesis of 7

Compound **6** (310.4 mg, 1.58 mmol) and iridium chloride hydrate (189 mg, 0.63 mmol) were dissolved in 2–ethoxyethanol (9 mL) and H_2O (3 mL). The mixture was refluxed for 24 h and cooled to room temperature. Then water (50 mL) was added and the resulting reddish orange precipitate was filtered to give a crude cyclometalated Ir(III) chlorobridged dimer with an isolated yield of 49 % (152.5 mg).

Synthesis of 1[34]

Compound **7** (96.5 mg, 0.08 mmol), acetylacetone (39.4 mg, 0.39 mmol) and Na_2CO_3 (41.3 mg, 0.39 mmol) were dissolved in 2–ethoxyethanol (1 mL) in a round–bottom flask. The mixture was heated and stirred at 50 °C for 1 h. The reaction mixture was then cooled down to room temperature, and extracted twice with CH_2Cl_2. The combined organic layer was dried over anhydrous Na_2SO_4 and filtered. Volatiles were removed under reduced pressure. The residue was purified by silica gel column chromatography with dichloromethane and methanol. The product was obtained after ether was added and the red orange solid was filtered with an isolated yield of 80 % (87.5 mg). ^{1}H NMR (300 MHz, DMSO–d_6, δ): 8.50 (d, J = 5.5 Hz, 2H), 8.31

(d, J = 8.0 Hz, 2H), 8.06 (t, J = 7.7 Hz, 2H), 7.85 (d, J = 8.1 Hz, 2H), 7.53 (t, J = 6.5 Hz, 2H), 7.38 (d, J = 8.0 Hz, 2H), 6.61 (s, 2H), 5.29 (s, 1H), 2.26 (s, 6H), 1.74 (s, 6H); ^{13}C NMR (75 MHz, DMSO–d_6, δ): 198.37, 184.77, 166.53, 150.64, 148.64, 147.13, 138.91, 136.18, 131.57, 124.37, 124.28, 121.98, 120.83, 100.91, 28.65, 26.86; HRMS (FAB) m/z: $[M]^+$ calc. for $C_{31}H_{27}IrN_2O_4$ 684.1600, found 684.1602.

Synthesis of 3[35]

Compound **7** (264.1 mg, 0.16 mmol), picolinic acid (60 mg, 0.49 mmol) and Na_2CO_3 (52 mg, 0.49 mmol) were dissolved in 2–ethoxyethanol (3 mL) in a round–bottom flask. The mixture was heated and stirred at reflux for 24 h. The reaction mixture was then cooled down to room temperature, and extracted with CH_2Cl_2. The organic layer was dried over anhydrous Na_2SO_4 and filtered. The residue was purified by silica gel column chromatography with dichloromethane and methanol. The product was obtained after ether was added and the orange solid was filtered with an isolated yield of 83 % (188.5 mg). ^{1}H NMR (300 MHz, DMSO–d_6, δ): 8.60 (d, J = 5.5 Hz, 1H), 8.39 (t, J = 7.0 Hz, 2H), 8.16–8.10 (m, 2H), 8.05 (d, J = 8.4 Hz, 2H), 8.01–7.93 (m, 2H), 7.71–7.60 (m, 3H), 7.53 (t, J = 6.1 Hz, 2H), 7.46 (dd, J = 8.1, 1.4 Hz, 1H), 7.37 (t, J = 6.5 Hz, 1H), 6.78 (s, 1H), 6.59 (d, J = 1.3 Hz, 1H), 2.32 (s, 3H), 2.26 (s, 3H); ^{13}C NMR (75 MHz, DMSO–d_6, δ): 198.35, 198.32, 172.17, 166.76, 165.98, 151.32, 149.98, 149.60, 149.54, 149.33, 148.77, 148.47, 146.99, 139.44, 139.10, 139.10, 137.14, 136.67, 131.16, 130.70, 129.69, 128.17, 125.17, 124.85, 124.82, 124.54, 122.59, 122.56, 121.27, 121.23, 26.96, 26.88; HRMS (FAB) m/z: $[M]^+$ calc. for $C_{32}H_{24}IrN_3O_4$ 707.1396, found 707.1398.

Synthesis of 5

A solution of dichlorobridged Ir dimer **7** (65 mg, 0.04 mmol) and silver tetrafluoroborate (19 mg, 0.1 mmol) in acetonitrile was refluxed for 12 h under nitrogen atmosphere. The AgCl formed as a by–product was removed through Celite® filtration. The resulting solution was evaporated then chromatographed over silica gel with acetonitrile as an eluent to give **5**. Yellow orange: Yield = 80 % (42 mg) ^{1}H NMR (400 MHz, CD_3CN, δ): 9.18 (m, 1H), 8.16 (m, 2H), 7.76 (d, J = 8.1 Hz, 1H), 7.60 (m, 1H), 7.47 (dd, J = 8.1, 1.7 Hz, 1H), 6.57 (d, J = 1.5 Hz, 1H), 2.25 (d, J = 3.4 Hz, 6H); ^{13}C NMR (75 MHz, CD_3CN, δ): 197.86, 165.57, 151.46, 149.25, 142.95, 139.43, 136.99, 129.81, 124.85, 124.16, 123.39, 121.02, 119.87, 25.79, 0.77; HRMS (FAB) m/z: $[M – BF_4^- – 2CH_3CN]^+$ calc. for $C_{26}H_{20}IrN_2O_2$ 585.1154, found 585.1155.

Synthesis of 8

Compound **8** was synthesized analogously to **7**, using phenylpyridine (271.6 mg, 1.75 mmol) instead of **6** and iridium chloride hydrate (200 mg, 0.7 mmol). Yield = 67 % (250 mg)

Synthesis of 2[36]

Compound **2** was synthesized analogously to **1**, using compound **8** (150 mg, 0.14 mmol) instead of **7** and acetylacetone (42 mg, 0.4 mmol). Yellow solid: Yield = 82 % (138 mg) ^{1}H NMR (300 MHz, DMSO–d_6, δ): 8.48 (d, J = 5.2 Hz, 2H), 8.13 (d, J = 8.0 Hz, 2H), 7.93 (dd, J = 11.1, 4.3 Hz, 2H), 7.68 (d, J = 7.5 Hz, 2H), 7.39 (t, J = 6.5 Hz, 2H), 6.77 (t, J = 7.1 Hz, 2H), 6.60 (t, J = 7.3 Hz, 2H), 6.07 (d, J = 7.4 Hz, 2H),

5.26 (s, 1H), 1.72 (s, 6H); ^{13}C NMR (75 MHz, DMSO–d_6, δ): 184.43, 168.02, 148.23, 147.86, 145.54, 138.36, 133.07, 128.80, 124.43, 122.92, 120.78, 119.33, 100.78, 28.70; HRMS (FAB) m/z: $[M]^+$ calc. for $C_{27}H_{23}IrN_2O_2$ 600.1389, found 600.1390.

Synthesis of 4[37]

Compound **4** was synthesized analogously to **3**, using compound **8** (30 mg, 0.03 mmol) instead of **7** and picolinic acid (10 mg, 0.08 mmol). Yellow solid: Yield = 80 % (29 mg) ^{1}H NMR (300 MHz, DMSO–d_6, δ): 8.53 (d, J = 5.4 Hz, 1H), 8.20 (t, J = 8.0 Hz, 2H), 8.15–8.04 (m, 2H), 7.96–7.86 (m, 2H), 7.81 (t, J = 8.2 Hz, 2H), 7.66 (d, J = 4.8 Hz, 1H), 7.58 (dd, J = 13.4, 5.8 Hz, 2H), 7.37 (t, J = 6.3 Hz, 1H), 7.21 (t, J = 6.3 Hz, 1H), 6.94–6.82 (m, 2H), 6.78 (t, J = 7.4 Hz, 1H), 6.71 (t, J = 7.3 Hz, 1H), 6.26 (d, J = 7.4 Hz, 1H), 6.07 (d, J = 7.3 Hz, H); ^{13}C NMR (75 MHz, DMSO–d_6, δ): 172.17, 168.27, 167.36, 151.55, 150.40, 148.75, 148.52, 148.10, 147.78, 145.06, 144.53, 139.15, 138.58, 138.58, 132.45, 132.25, 130.12, 129.44, 129.44, 128.03, 125.29, 124.69, 123.76, 123.43, 121.63, 121.38, 119.82, 119.74; HRMS (FAB) m/z: $[M]^+$ calc. for $C_{28}H_{20}IrN_3O_2$ 623.1185, found 623.1186.

B.1.5. Supporting Information

Single Crystal X–ray Diffraction Studies

Single crystals of $C_{26}H_{22}IrN_4$ $[(ppy)_2Ir(CH_3CN)_2]$ were grown by slow vaporization method. A suitable crystal was selected onto a nylon loop with Paratone® N oil and mounted on Agilent SuperNova, Dual, Cu at home/near, AtlasS2 diffractometer. The crystal was kept at 293.0(4) K during data collection using Cu Kα radiation (λ= 1.542

Å). A total number of 10459 reflections were measured (6.078° ≤ 2θ ≤ 147.946°) with 1° steps (ω scan). The structure was solved with *ShelXT* software using direct methods and refined using least squares minimization refinement package of OLEX2. CCDC 1576742 contains the supplementary crystallographic data of this paper. These data can be obtained free of charge from the Cambridge Crystallographic Data Centre via www.ccdc.cam.ac.uk/data_request/cif.

Table 1. Crystallographic Data and Structure Refinement Information for $(ppy)_2Ir(CH_3CN)_2$.

Identification code	$(ppy)_2Ir(CH_3CN)_2$
Empirical formula	$C_{26}H_{22}IrN_4$
Formula weight	582.67
Temperature/K	293.0(4)
Crystal system	monoclinic
Space group	$P2_1/c$
a/Å	14.9543(4)
b/Å	20.0441(5)
c/Å	9.0693(2)
α/°	90
β/°	103.535(3)
γ/°	90
Volume/Å^3	2642.98(12)
Z	4
ρ_{calc}/g/cm^3	1.464
μ/mm^{-1}	9.905
F(000)	1132
Crystal size/mm^3	0.1 × 0.05 × 0.05
Radiation	CuKα (λ = 1.54184)
2θ range for data collection/°	6.078 to 147.946
Index ranges	$-18 \leq h \leq 18$, $-20 \leq k \leq 24$, $-11 \leq l \leq 7$
Reflections collected	10459

Independent reflections	5203 [R_{int} = 0.0220, R_{sigma} = 0.0253]
Data/restraints/parameters	5203/0/258
Goodness–of–fit on F^2	1.07
Final R indexes [$I \geq 2\sigma$ (I)]	R_1 = 0.0346, wR_2 = 0.0949
Final R indexes [all data]	R_1 = 0.0385, wR_2 = 0.0977

B.2. Electrogenerated Chemiluminescence Probes

B.2.1. Results and Discussion

ECL property

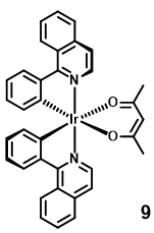

9

We further designed and synthesized an Ir(III) complex possessing 1–phenylisoquinoline (piq) groups as main ligands (**9**), which is well known for exhibiting better ECL property than Ir(III) complexes possessing 2–phenylpyridine (ppy) groups as main ligands. This phenomenon is due to the difference of LUMO energy levels of Ir(III) complexes, which should be lower than the LUMO of TPA radical for efficient electron transfer. Isoquinoline, which is a stronger electron–withdrawing group than pyridine stabilizes the LUMO level, resulting in better electron transfer followed by the formation of the excited state.[38]

As predicted, among three Ir(III) complexes (**1**, **2**, **9**), the probe **9** showed the highest ECL intensity and turn–off ratio (Fig. 17). Therefore, further ECL experiments were mainly conducted with **9**.

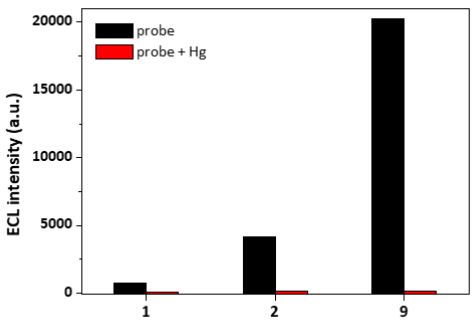

Figure 17. Comparison of ECL intensities of **1**, **2** and **9** before and after the addition of Hg^{2+} ion (80 μM) in CH_3CN/water (9/1).

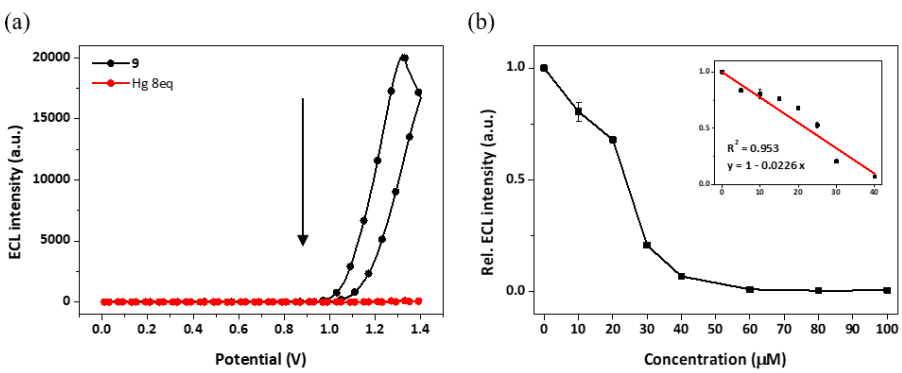

Figure 18. (a) ECL intensity of 10 μM of **9** upon the addition of Hg^{2+} in CH_3CN/water (9/1 v/v, 30 mM TPA, and 0.1 M TBAP as a supporting electrolyte). The potential was swept at a Pt disk electrode (diameter: 2 mm) over the range 0–1.4 V vs Ag/AgCl (scan rate: 0.1 V/s). (b) ECL intensity of 10 μM of **9** upon the addition of Hg^{2+} showing the linearity.

ECL measurements were performed in acetonitrile/water = 9/1 solution mixture of 10 μM of **9** and 30 mM of TPA as a coreactant with 0.1 M TBAP as a

supporting electrolyte. As shown in Fig. 18, the ECL intensity decreased gradually until the concentration of mercury(II) ion reached 40 μM. A good linear relationship was observed over the range of 0–40 μM and the estimated limit of detection was 170 pM (signal–to–noise (S/N) ratio=3, n=3).

1 and **2** as well showed the decrement of the ECL intensity until 80 μM of mercury(II) ion was added (Fig. 19). In this case, a double amount of mercury(II) ion were needed for saturation compared to **9**. Interestingly, the ECL intensity of **1** decreased exponentially upon the addition of mercury(II) ion. The estimated limit of detection was 1.9 nM and 0.78 nM for **1** and **2**, respectively, which appear to be much smaller than the LOD determined by photoluminescence.

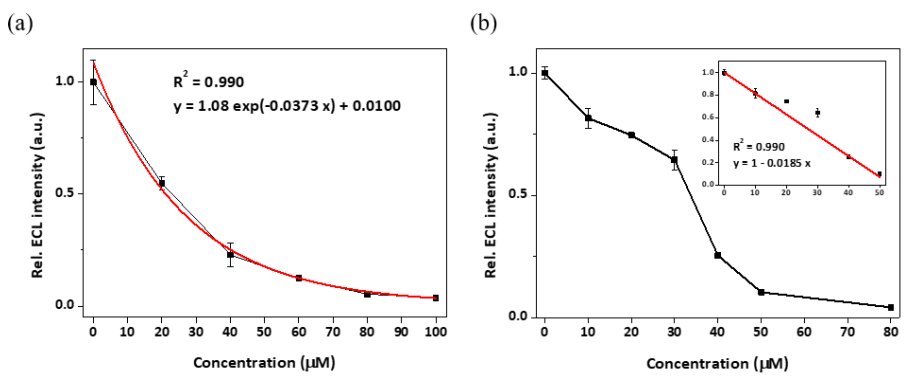

Figure 19. (a) ECL intensity of 10 μM of **1** upon addition of Hg^{2+} ion (0–100 μM) in CH_3CN/water (9/1 v/v, 100 mM TPA, and 0.1 M TBAP as the supporting electrolyte). The potential was swept at a Pt disk electrode (diameter: 2 mm) over the range 0–1.8 V vs Ag/AgCl (scan rate: 0.1 V/s). LOD = 1.9 nM. (b) ECL intensity of 10 μM of **2** upon the addition of Hg^{2+} ion (0–80 μM) in CH_3CN/water (9/1 v/v, 30 mM TPA, and 0.1 M TBAP as the supporting electrolyte). The potential was swept at a Pt disk electrode (diameter: 2 mm) over the range 0–1.4 V vs Ag/AgCl (scan rate: 0.1 V/s). Inset: Plot of ECL intensity vs [Hg^{2+}] (0–50 μM) showing the linear relationship. LOD = 0.78 nM.

Selectivity Test

A selective binding assay of **9** was carried out as shown in Fig. 20. The ECL intensity certainly decreased only in the presence of mercury(II) ion. Other various metal ions (50 μM), such as Ag^{+}, Al^{3+}, Ca^{2+}, Cd^{2+}, Co^{2+}, Cu^{2+}, Fe^{2+}, K^{+}, Mg^{2+}, Mn^{2+}, Na^{+}, Ni^{2+}, Pb^{2+}, and Zn^{2+}, resulted in small changes in the ECL intensities of **9**.

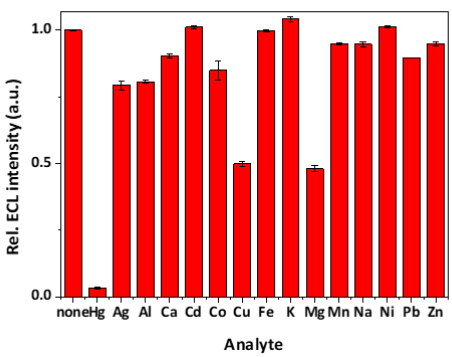

Figure 20. ECL responses of **9** (10 μM) in the presence of 50 μM of Hg^{2+} ion and various metal ions in CH_3CN/water (9/1).

Cyclic Voltammetry

The probes **1**, **2** and **9** showed ECL quenching in the presence of mercury(II) ion. This phenomenon might be inevitable as the ECL process can occur only when proper oxidation is allowed. However, the results of cyclic voltammetry (CV) showed that after the addition of mercury(II) ion, no significant oxidation peaks were observed compared to the CVs before adding mercury(II) ion (Fig. 21). Therefore,

we can conclude that the proper oxidation does not occur after the addition of mercury(II) ion, which manifests as a suppression of the ECL intensity.

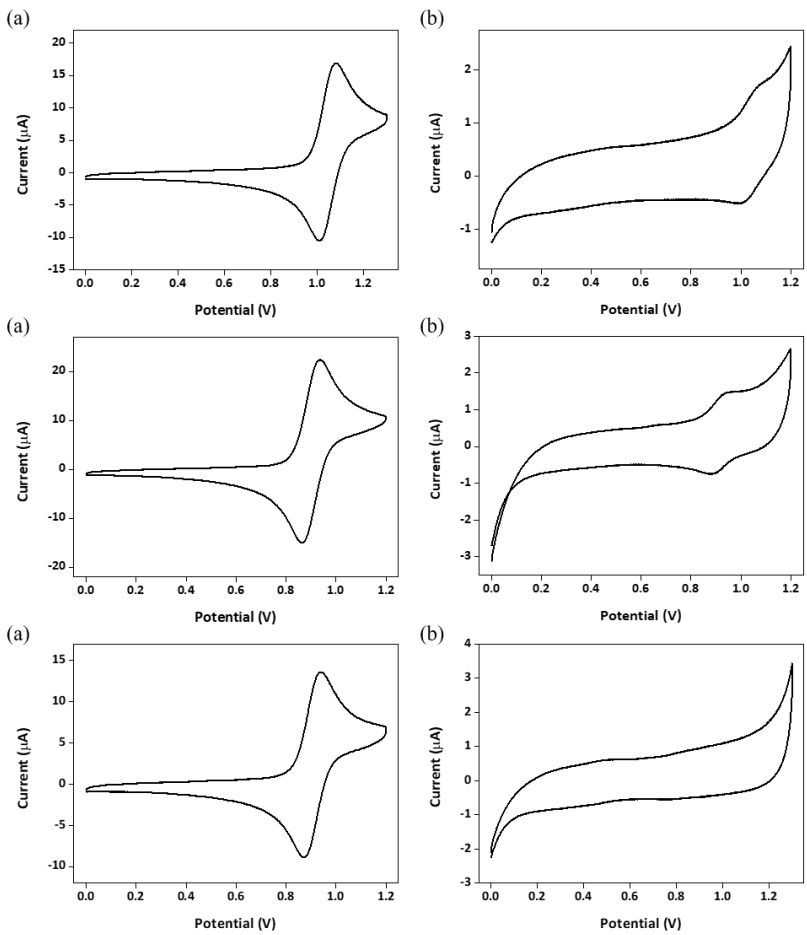

Figure 21. Cyclic voltammogram of (a) **1**, (b) **1** + Hg^{2+} (1 equivalent), (c) **2**, (d) **2** + Hg^{2+} (1 equivalent), (e) **9**, (f) **9** + Hg^{2+} (1 equivalent) in CH_3CN.

B.2.2. Conclusion

We developed a series of Ir(III) complexes possessing acetylacetonate ancillary ligands. After the addition of mercury(II) ion, the ECL intensities of the probes **1**, **2** and **9** were suppressed instantaneously. Especially, the observed ECL turn−off ratio of **9** was remarkable compared to **1** and **2** owing to the proper LUMO energy level of phenylisoquinoline.

B.2.3. Experimental Section

Electrochemical and electrochemiluminescent measurements

Electrochemical study was performed with a CH Instruments 650B Electrochemical Analyzer (CH Instruments, Inc., TX, USA). ECL spectra were gained using a charge–coupled device (CCD) camera (LN/CCD 1752–PB/VSAR, Princeton Instruments, NJ, USA) which is maintained below −120 °C using liquid N_2. The ECL intensity profile was obtained using a low–voltage photomultiplier tube (PMT) module (H–6780, Hamamatsu photonics K. K., Tokyo, Japan) operated at 1.4 V. A 250 μL–sized ECL cell was directly mounted on the CCD or PMT module with home–made mounting support during the experiments. All the ECL data were collected via simultaneous cyclic voltammetry. The ECL solutions commonly contained tri(*n*–propyl)amine (TPA, Sigma–Aldrich, MO, USA) as a coreactant and 0.1 M tetrabutylammonium perchlorate (TBAP, TCI) as a supporting electrolyte in acetonitrile (CH_3CN, spectroscopy grade, ACROS). Especially, TPA was selected as it has been widely studied and known on its electrochemical properties. The ECL measurements were carried out under ambient conditions. The electrochemical measurements were referenced with respect to an Ag/Ag^+ reference electrode in organic solvents, or to an Ag/AgCl in aqueous media. Especially, the potential values measured under organic conditions were calibrated against the saturated calomel electrode (SCE) using ferrocene as an internal reference ($E^o(F_c^+/F_c)$ = 0.424 V vs SCE). Pt working electrode was polished with 0.05 M alumina (Buehler, IL, USA) on a felt pad followed by sonication in 1:1 mixed solution of deionized water and absolute ethanol for 5 min. Then it was dried by ultra–pure N_2 gas for 1 min. All the solutions were not reused. The reported ECL values were obtained by averaging the values of at least three repetitive experiments with a good reliability. Cyclic

voltammetry (CV) was applied to individual solutions in order to investigate electrochemical oxidative and reductive behaviors.

Synthesis of compounds

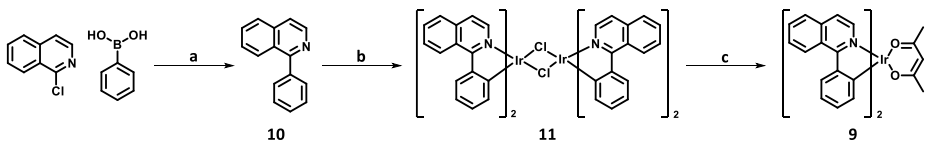

Scheme 3. a) $Pd(PPh_3)_4$, K_2CO_3, THF, H_2O, reflux; b) $IrCl_3 \cdot xH_2O$, 2–ethoxyethanol, H_2O, reflux; c) acetylacetone, Na_2CO_3, 2–ethoxyethanol, 50 °C. (THF = tetrahydrofuran)

Synthesis of 10

1–chloroisoquinoline (1000 mg, 6.1 mmol), boronic acid (964 mg, 7.9 mmol), tetrakis(triphenyl phosphine)palladium (208 mg, 0.18 mmol) and K_2CO_3 (2480 mg, 18 mmol) were dissolved in THF (30 mL) and H_2O (30 mL). The mixture was refluxed at 80 °C for 5 h and was cooled down to room temperature. The residue was extracted with CH_2Cl_2 and the organic layer was dried over anhydrous Na_2SO_4, filtered and evaporated under reduced pressure to afford the crude product. Then it was purified by silica gel column chromatography with hexane and ethyl acetate. The product was obtained as a white solid with an isolated yield of 93 % (1170 mg). ^{1}H NMR (300 MHz, $CDCl_3$, δ): 8.64 (d, J = 5.7 Hz, 1H), 8.13 (d, J = 8.5 Hz, 1H), 7.90 (d, J = 8.2 Hz, 1H), 7.65–7.75 (m, 4H), 7.50–7.59 (m, 4H).

Synthesis of 11

Compound **10** (1170 mg, 5.7 mmol) and iridium chloride hydrate (682 mg, 2.28 mmol) were dissolved in 2–ethoxyethanol (18 mL) and H_2O (6 mL). The mixture was refluxed for 24 h and cooled to room temperature. Then water was added and the resulting reddish orange precipitate was filtered to give a crude cyclometalated Ir(III) chlorobridged dimer with an isolated yield of 70 % (1035 mg).

Synthesis of 9[39]

Compound **11** (500 mg, 0.38 mmol), acetylacetone (115 mg, 1.15 mmol) and Na_2CO_3 (196 mg, 1.85 mmol) were dissolved in 2–ethoxyethanol (5 mL) in a round–bottom flask. The mixture was heated and stirred at 50 °C for 1 h. The reaction mixture was then cooled down to room temperature, and extracted twice with CH_2Cl_2. The combined organic layer was dried over anhydrous Na_2SO_4 and filtered. Volatiles were removed under reduced pressure. The residue was purified by silica gel column chromatography with dichloromethane and methanol. The product was obtained after ether was added and the red orange solid was filtered with an isolated yield of 78 % (440 mg). ^{1}H NMR (400 MHz, DMSO–d_6, δ): 8.95 (d, J = 8.0 Hz, 2H), 8.34 (d, J = 6.4 Hz, 2H), 8.19 (d, J = 8.0 Hz, 2H), 8.14–8.09 (m, 2H), 7.82 (m, 6H), 6.84 (t, J = 7.1 Hz, 2H), 6.56 (t, J = 7.2 Hz, 2H), 6.12 (d, J = 7.1 Hz, 2H), 5.25 (s, 1H), 1.67 (s, 6H); ^{13}C NMR could not be obtained because of poor solubility; HRMS (FAB) m/z: $[M]^+$ calc. for $C_{35}H_{27}IrN_2O_2$ 700.1702, found 700.1704.

References

1. Martinez–Manez, R.; Sancenon, F. *Chem. Rev.* **2003**, *103*, 4419–4479.
2. Snowden, T. S.; Anslyn, E. V. *Curr. Opin. Chem. Biol.* **1999**, *3*, 740–746.
3. Ueno, T.; Urano, Y.; Setsukinai, K. –I.; Takakusa, H.; Kojima, H.; Kikuchi, K.; Ohkubo, K.; Fukuzumi, S.; Nagano, T. *J. Am. Chem. Soc.* **2004**, *126*, 14079–14085.
4. Yuan, L.; Lin, W.; Zheng, K.; Zhu, S. *Acc. Chem. Res.* **2013**, *46*, 1462–1473.
5. Richter, M. M. *Chem. Rev.* **2004**, *104*, 3003–3036.
6. Hercules, D. M. *Science*, **1964**, *145*, 808.
7. Visco, R. E.; Chandross, E. A. *J. Am. Chem. Soc.* **1964**, *86*, 5350.
8. Santhanam, K. S. V.; Bard, A. J. *J. Am. Chem. Soc.* **1965**, *87*, 139.
9. Miao, W. *Chem. Rev*. **2008**, *108*, 2506–2553.
10. *Electrogenerated Chemiluminescence*; Bard, A. J. Ed.; Dekker: New York, 2004.
11. Rubinstein, I.; Bard, A. J. *J. Am. Chem. Soc.* **1981**, *103*, 512.
12. Miao, W.; Choi, J. –P.; Bard, A. J. *J. Am. Chem. Soc.* **2002**, *124*, 14478–14485.
13. Leland, J. K.; Powell, M. J. *J. Electrochem. Soc.* **1990**, *137*, 3127–3131.
14. Quang, D. T.; Kim, J. S. *Chem. Rev.* **2010**, *110*, 6280–6301.
15. Kim, H. N.; Ren, W. X.; Kim, J. S.; Yoon, J. *Chem. Soc. Rev.*, **2012**, *41*, 3210–3244.
16. Nolan, E. M.; Lippard, S. J. *Chem. Rev.* **2008**, *108*, 3443–3480.
17. Sancenon, F.; Martinez–Manez, R.; Soto, J. *Angew. Chem. Int. Ed.* **2002**, *41*, 1416–1419.
18. Prodi, L.; Bargossi, C.; Montaliti, M.; Zaccheroni, N.; Su, N.; Bradshaw, J. S.; Izatt, R. M.; Savage, P. B. *J. Am. Chem. Soc.* **2000**, *122*, 6769–6770.
19. Song, F.; Watanabe, S.; Floreancig, P. E.; Koide, K. *J. Am. Chem. Soc.* **2008**, *130*, 16460–16461.
20. Lee, D. –N.; Kim, G. –J.; Kim, H. –J. *Tetrahedron Lett.* **2009**, *50*, 4766–4768.

21. Han, D.; Kim, Y. –R.; Oh, J. –W.; Kim, T. H.; Mahajan, R. K.; Kim, J. S.; Kim, H. *Analyst*, **2009**, *134*, 1857–1862.
22. You, Y.; Nam, W. *Chem. Soc. Rev.* **2012**, *41*, 7061–7084.
23. You, Y.; Park, S. Y. *J. Am. Chem. Soc.* **2005**, *127*, 12438–12439.
24. Maity, A.; Sil, A.; Nad, S.; Patra, S. K. *Sens. and Actuators, B*, **2018**, *255*, 299–308.
25. Bonati, F.; Minghetti, G. *J. Organometal. Chem.* **1970**, *22*, 5–10.
26. Flatau, K.; Musso, H. *Angew. Chem. Int. Ed.* **1970**, *9*, 379–380.
27. Allmann, R.; Flatau, K.; Musso, H. *Chem. Ber.* **1972**, *105*, 3067–3077.
28. Fish, R. H.; Lundin, R. E.; Haddon, W. F. *Tetrahedron Lett.* **1972**, *10*, 921–924.
29. Zeng, H.; Yu, F.; Dai, J.; Sun, H.; Lu, Z.; Li, M.; Jiang, Q.; Huang, Y. *Dalton Trans.* **2012**, *41*, 4878–4883.
30. Mei, Q.; Shi, Y.; Chen, C.; Hua, Q.; Tong, B. *Inorg. Chem. Commun.* **2016**, *73*, 147–151.
31. Dolomanov, O. V.; Bourhis, L. J.; Gildea, R. J.; Howard, J. A. K.; Puschmann, H. OLEX2: A complete structure solution, refinement and analysis program. *J. Appl. Cryst.* **2009**, *42*, 339–341.
32. Olivier, J. –H.; Harrowfield, J.; Ziessel, R. *Chem. Commun.* **2011**, *47*, 11176–11188.
33. Bonati, F.; Minghetti, G. *Angew. Chem. Int. Ed.* **1968**, *7*, 629–630.
34. Lee, K. H.; Kang, H. J.; Lee, S. J.; Seo, J. H.; Kim, Y. K.; Yoon, S. S.; *Synth. Met.* **2011**, *161*, 1113–1121.
35. Wang, D.; Wu, Y.; Jiao, B.; Dong, H.; Zhou, G.; Wang, G.; Wu, Z.; *Org. Electron.* **2013**, *14*, 2233–2242.
36. Nazeeruddin, Md. K.; Humphry–Baker, R.; Berner, D.; Rivier, S.; Zuppiroli, L.; Grätzel, M. *J. Am. Chem. Soc.* **2003**, *125*, 8790–8797.

37. McDonald, A. R.; Mores, D.; Donega, C. de M.; Walree, C. A.; Gebbink, R. J. M. K.; Lutz, M.; Spek, A. L.; Meijerink, A.; Klink, G. P. M.; Koten, G. *Organometallics*, **2009**, *28*, 1082–1092.
38. Kim, H. J.; Lee, K. –S.; Jeon, Y. –J.; Shin, I. –S.; Hong, J. –I. *Biosens. Bioelectron.* **2017**, *91*, 497–503.
39. Yang, C. –H.; Tai, C. –C.; Sun, I. –W. *J. Mater. Chem.* **2004**, *14*, 947–950.

국문 초록

독성이 매우 큰 물질로 널리 알려진 수은 이온은 인체의 건강과 환경에 심각한 위험을 초래한다. 따라서 수은 이온을 효과적으로 검출하기 위한 다양한 화학 센서의 개발이 이루어져왔다. 그러나 비용적인 측면에서 효율적이며 수은 이온을 신속하고 선택적으로 검출할 수 있는 센서의 개발은 여전히 시급한 실정이다.

본 연구에서 우리는 고리형 이리듐 복합체를 기반으로 하는 인광 및 전기화학 발광의 센서를 개발하였다. 페닐피리딘 또는 페닐아이소퀴놀린을 주리간드로 가지며 공통적으로 아세틸아세톤을 보조리간드로 가지는 이리듐 착물들을 합성하여 아세틸아세톤이 수은 이온과 선택적으로 반응하도록 유도하였다.

프로브 **1** 의 아세틸아세톤은 수은 이온과 선택적으로 반응하여 인광이 증가하는 동시에 청색 편이가 일어났다. 한편, 프로브 **2** 의 경우 수은 이온과 반응 후에 인광이 감소하는 경향을 보였다. 또한 수은 이온 첨가 전 후의 NMR 스펙트럼을 비교함으로써 두 단계에 걸친 검출 메커니즘을 밝혀내었다. 추가적으로 질량 및 결정 분석을 통해서 아세틸아세톤이 수은 이온과 반응한 후 아세틸아세톤이 이리듐 착물로부터 떨어져 나간다는 사실을 증명하였다.

이 프로브들은 수은 이온의 첨가에 의해 전기화학적 발광 (ECL)이 감소하는 경향을 나타내었다. ECL 기반의 화학 센서는 현장 진단 검출에 사용될 수 있는 가능성이 있으며 고감도, 간단한 분석 등 다양한 장점을 가지고있다. 그 중에서도 프로브 **9** 는 특히 가장 우수한 ECL 특성을 보였으며 수은 이온 농도 0–40 μM 의 구간에서 선형 관계를 나타내었고 검출 한계는 170 pM 로 매우 낮은 측정값을 보였다.

주요어: 고리형 이리듐 복합체, 아세틸아세톤, 키모도시미터, 인광, 전기화학적 발광 (ECL), 듀얼 모드, 수은 이온

학번: 2016-20358